Journal of Applied Polymer Science

High-efficiency recovery of rare earth ions by hydrolyzed poly(styrene-*co*-maleic anhydride)

Wenjun Gui,[1] Ying Yang,[1,2] Xuan Zhu[1]

[1]Department of Chemistry and Chemical Engineering, Lanzhou University, Lanzhou 730000, People's Republic of China

[2]Key Laboratory of Nonferrous Metals Chemistry and Resources Utilization of Gansu Province, Lanzhou 730000, People's Republic of China

Correspondence to: Y. Yang (E-mail: yangying@lzu.edu.cn)

ABSTRACT: Hydrolyzed poly(styrene-*co*-maleic anhydride) (PSMA) as a high-efficiency adsorbent is used for recovering La^{3+}, Eu^{3+}, Tb^{3+}, and Yb^{3+} from the simulate wastewater of bastnaesite leach liquor. The pseudo-first-order and pseudo-second-order models are used to fit adsorption data in the kinetic studies and the results show good correlation with the pseudo-second-order model. The Langmuir model is found to fit for the isotherm data of all the rare earth ions (RE^{3+}) and the maximum adsorption capacity of hydrolyzed PSMA is 285.79, 301.92, 305.46, and 336.65 mg g^{-1} at 298 K for La^{3+}, Eu^{3+}, Tb^{3+}, and Yb^{3+}, respectively. The adsorption could be conducted in at pH 6.0 and the equilibrium is fast established in 30 min. Competition from coexisting ions (Ca^{2+}, Mg^{2+}) was proved to be insignificant. Moreover, the spent adsorbent could be well regenerated and kept above 80% of adsorption efficiency at the end of the fifth cycle. © 2016 Wiley Periodicals, Inc. J. Appl. Polym. Sci. **2016**, *133*, 43676.

KEYWORDS: adsorption; copolymers; kinetics; rare earth ions

Received 3 November 2015; accepted 21 March 2016

DOI: 10.1002/app.43676

INTRODUCTION

In recent times, rare earth (RE) and related materials have garnered much prominence due to their essential role in permanent magnets, lamp phosphors, rechargeable NiMH batteries, catalysts for petroleum cracking, metallurgy, glass and ceramics.[1,2] Tens of thousands of tons of rare earth are consumed for global industries annually. However, there is a shortfall in supply of rare earth because of its scarce resources. Meanwhile, in the separation process of rare earth, a large volume of wastewater containing the low concentration RE is discharged, causing a part of rare earth waste. Many potential water sources containing this wastewater could pollute the environment. In addition, the rare earth usually gets into the environment in biologically available forms, and may enter the human body through food chains which causes harm to health. Once La(III) and Gd(III) ions enter the neurons, they will interfere with calcium channels in human and animal cells, and also alter or even inhibit the action of various enzymes and regulate synaptic transmission.[3–5] Therefore, the cleaner methods of recovering rare earth are always more desirable to reduce environmental pollution in industry.

Some typical approaches for enrichment rare earth include ion-exchange,[6,7] extraction,[8–13] precipitation,[14] chromatography,[15,16] and adsorption.[17–19] The adsorption is a promising technique because of its wide raw material sources, simple operation, easy recovery and high effectiveness. Many inorganic and organic materials have been applied for removing metal ions. Specifically, polymeric adsorbent are widely used in modern adsorption separation technology due to their favorable physicochemical stability, large adsorption capacity, excellent selectivity, and structural diversity.[20,21] For instance, poly(acrylamide-expanded perlite), a novel composite, was synthesized for the enrichment of Tb(III) ions,[22] and magnetic nanocomposite hydrogel with ZnO-initiated photopolymerization adsorbed La(III) ions.[23]

In our previous work, we have reported the synthesis of macromolecular metal complexes (MMC) containing thorium with polymeric ligands, and this process can be used for recovery radioactive element Th.[24] As part of our continuing investigation into the development of above work, herein we describe hydrolyzed poly(styrene-*co*-maleic anhydride) (PSMA) as a high-efficiency adsorbent for enrichment RE^{3+} from the simulate wastewater of bastnaesite treatment process. Bastnaesite is one of the main sources of rare earth elements in China. At present, exploitation processing of this ore involves oxidation roasting, sulfuric acid leaching of rare-earth oxide, and precipitation sodium RE double sulfates to obtaining a crude separation into light and heavy fractions.[25–27] During this process, a

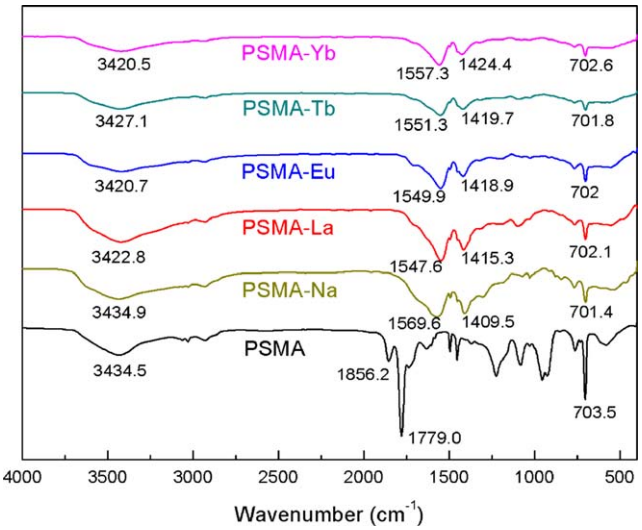

Figure 1. FTIR spectra of the PSMA, PSMA-Na, PSMA-La, PSMA-Eu, PSMA-Tb and PSMA-Yb. [Color figure can be viewed in the online issue, which is available at wileyonlinelibrary.com.]

large amount of wastewater containing low content rare earth elements and light metals (such as Ca^{2+} and Mg^{2+}) was produced. Our study aims to recover the highly valuable and potentially harmful rare earth under competitive conditions. Hydrolyzed PSMA acts as a bidentate ligand coordinated to the RE^{3+}. In contrast, the hydrolyzed PSMA adsorbs light metals slightly. After adsorption, the concentration of the rare earth in solution meets the national discharge standard (GB26451-2011). The adsorption mechanism and conditions are investigated. The PSMA resin is one of the promising candidates for efficiently separating rare earth ions from the wastewater of bastnaesite leach liquor.

EXPERIMENTAL

Chemicals

La_2O_3 and Yb_2O_3 were purchased from Tianjin Guangfu Fine Chemical Research Institute. Eu_2O_3 and Tb_2O_3 were purchased from Shanghai Zhongtai Reagent Company Limited. Stock solutions of La^{3+}, Eu^{3+}, Tb^{3+}, and Yb^{3+} were prepared by their oxides dissolved in 0.10 mol L^{-1} aqueous sulfuric acid. Other reagents were of analytical reagent grade.

Preparation of Hydrolyzed PSMA

The PSMA resin was prepared according to our previous works.[28] 1.0691 g of PSMA was added in 500 mL of 0.9372 g L^{-1} dilute sodium hydroxide solution. Then the mixture was stirred at ambient temperature until it dissolved completely. The hydrolyzed product (PSMA-Na) was obtained. The molar concentrate of maleic anhydride in solution (C_{MA}) was determined by back titration method. It was calculated using eq. (1):

$$C_{MA}(\text{mol L}^{-1}) = \frac{CV - C_1 V_1}{2V_1} \quad (1)$$

where MA is maleic anhydride, V is the volumes (L) of sodium hydroxide aqueous solution before hydrolysis. V_1 is the total volumes (L) of solution after alkaline hydrolysis. C is the concentration of sodium hydroxide aqueous solution (mol L^{-1}) before hydrolysis. C_1 is the concentration of residual sodium hydroxide aqueous solution (mol L^{-1}) after hydrolysis. Thus, the molar concentrate of maleic anhydride in solution is 0.0067 mol L^{-1} and the content of maleic anhydride in PSMA is 30.71%.

Characterization of Chelating Adsorbent

FTIR spectra were recorded on a Thermo Nicolect Mattson 2110 spectrometer from 4000 to 400 cm^{-1} using KBr disks. The scanning electron microscopy (SEM) images were taken with a field-emission scanning electron microscope (JEOLJSM-6701F). The metal ions (RE^{3+}, Ca^{2+}, and Mg^{2+}) in solution were determined by inductively coupled plasma atomic emission spectrometry (POEMSI, Thermo Jarrell Ash Corp). The concentrations of RE^{3+} in solution were measured in a JASCO UV–Vis (model V-530) spectrophotometer. The X-ray photoelectron spectroscopy (XPS) were recorded using a Kratos Axis Ultra DLD spectrometer (Kratos Analytical-A Shimadzu Group Company, Japan) with monochromatic Al–Kα radiation as the excitation and an X-ray power of 600 W.

Adsorption Experiments

The adsorption of RE^{3+}, including La^{3+}, Eu^{3+}, Tb^{3+}, and Yb^{3+}, on hydrolyzed PSMA in aqueous solution were investigated in a series of adsorption experiments. At room temperature, 5.5 mL of the hydrolyzed PSMA solution was added into a 6.7 mL of 0.0025 mol L^{-1} $RE_2(SO_4)_3$ aqueous solution at pH of 6.0. Then the mixture was stirred for 2 h to ensure adsorption equilibrium. After adsorption experiments, the PSMA-RE precipitates were isolated from the solution by centrifugation and the equilibrium concentration of rare earth ions in solution were determined by UV–Vis spectrophotometer at 650 nm using arsenazo (III).

To determine adsorption kinetics, the initial test solution was sampled at various time intervals (3, 6, 9, 15, 20, 30, 40, 60, 90, and 120 min) and at 298.15 K. In adsorption isotherms study, solution with various initial concentration (20, 30, 35, and 40 mg L^{-1}) of individual metal ion were treated at diffident temperature (298, 308 and 318K). In the effect of pH, the pH value of solution was adjusted by adding either 0.1 mol L^{-1} NaOH or 0.1 mol L^{-1} HCl. The amount of RE^{3+} adsorbed on hydrolyzed PSMA at adsorption equilibrium according to the following (2) and (3):

$$q = \frac{(C_0 - C_e)V_{ad}}{W} \quad (2)$$

$$\text{Adsorption\%} = \frac{C_0 - C_e}{C_0} \times 100 \quad (3)$$

where q is the adsorption capacity (mg g^{-1}), C_0 and C_e are the initial and equilibrium concentration of the adsorbate (mg L^{-1}), respectively. V_{ad} (L) is the volume of the solution used for adsorption and W(g) is the weight of the adsorbent.

For the competitive experiment, the certain amount of adsorbent was shaken with the mixture solution containing 20 mg L^{-1} RE^{3+} and 100 mg L^{-1} Ca^{2+} or 50 mg L^{-1} Mg^{2+} for 2 h in a binary component system. After the competitive adsorption, the residual RE(III) ions in solution were analyzed via the ICP. The

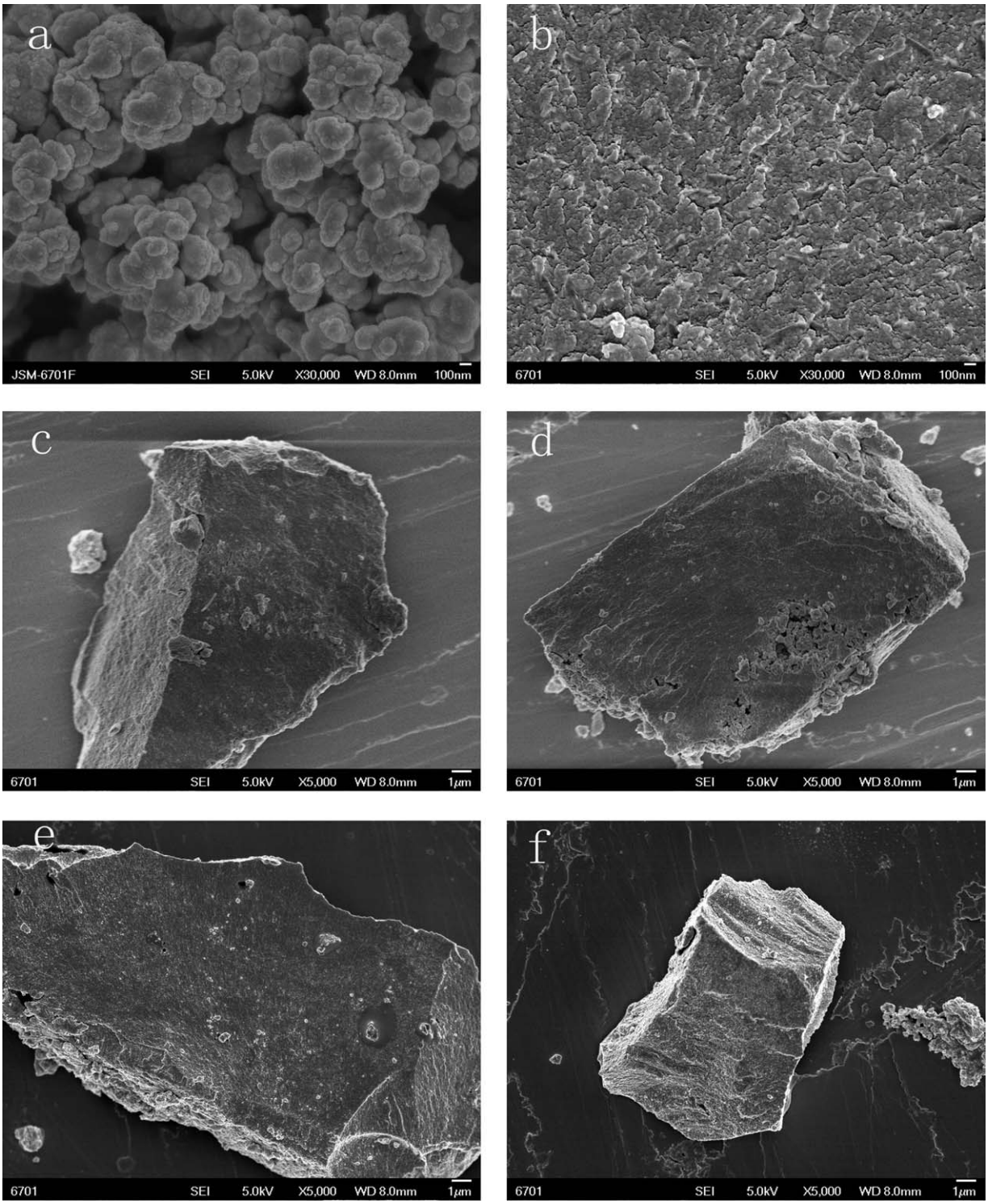

Figure 2. SEM images of PSMA (a), PSMA-Na (b), PSMA-La (c), PSMA-Eu (d), PSMA-Tb (e), and PSMA-Yb (f).

selectivity coefficient (β) was calculated using the following eq. (4):

$$\beta = \frac{C_{RE}\, C_{alka(aq)}}{C_{RE(aq)}\, C_{alka}} \tag{4}$$

where C_{RE} and C_{alka} (Ca and Mg are all alkaline earth element) are the concentrations of the metals in the phase of the resin, and $C_{RE(aq)}$ and $C_{alka(aq)}$ are the concentrations of the metals in solution at equilibrium.[29]

Desorption and Regeneration Studies

Acidic solutions have been widely used for desorbing the heavy metal ions from resin.[30–32] The experiments of desorption were performed with 0.1, 0.5, and 1 mol L^{-1} HCl aqueous solution

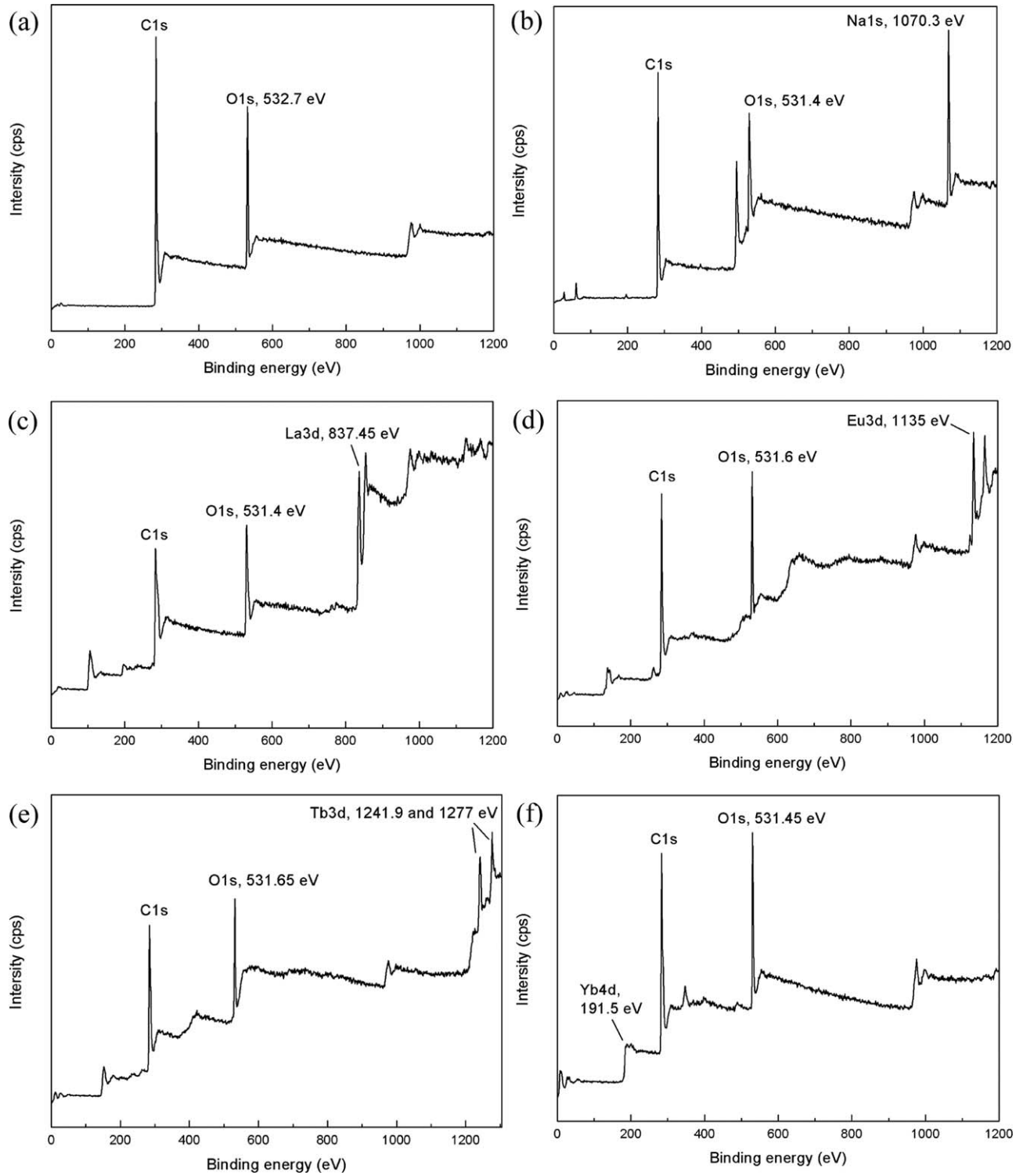

Figure 3. XPS spectra of: PSMA (a), PSMA-Na (b), PSMA-La (c), PSMA-Eu (d), PSMA-Tb (e), and PSMA-Yb (f).

after hydrolyzed PSMA was equilibrated with RE^{3+}. The PSMA-RE was put into the acidic solution for 24 h, and then the acidification of the resin (white precipitates) was obtained, washing with distilled water until it was neutral. After desorption, the resin was regenerated in 0.02 mol L^{-1} NaOH aqueous solution and reused in the next cycle of adsorption experiment. The desorption efficiency (D_e) was calculated using eq. (5):

$$D_e\% = \frac{C_d V_d}{(C_0 - C_e) V_{ad}} \times 100 \quad (5)$$

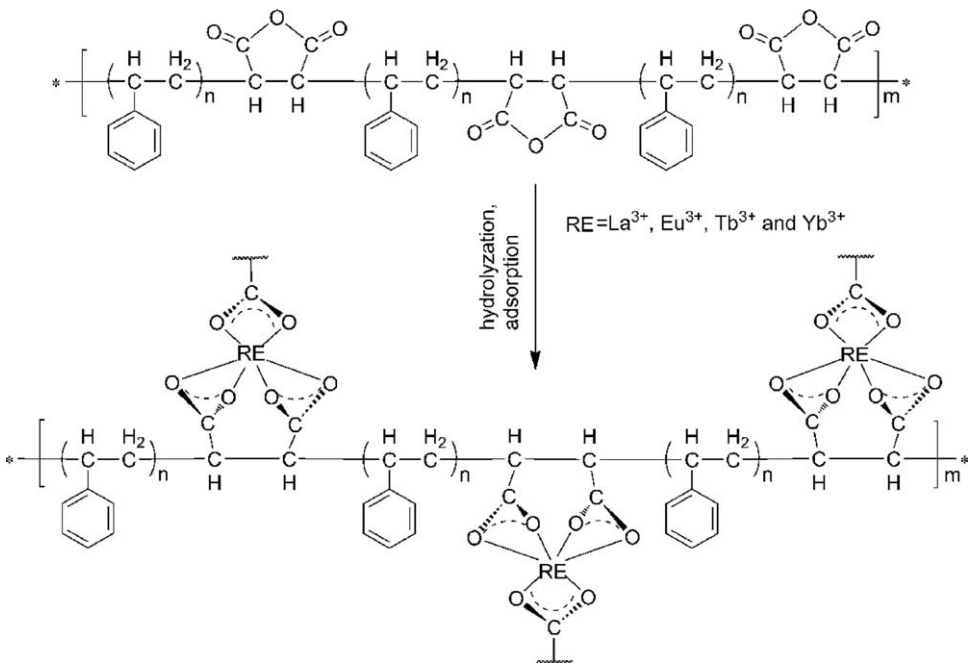

Scheme 1. The proposed adsorption mechanisms of RE (III) ions on PSMA.

where C_d is the concentration of RE^{3+} in the eluent solutions (mg L^{-1}), V_d is the volume of the desorption solution, C_0, C_e, and V_{ad} are the same as defined above.

RESULTS AND DISCUSSION

Characterization of PSMA, PSMA-Na, and PSMA-RE

The FTIR spectra of PSMA, PSMA-Na, and PSMA-RE are presented in Figure 1. A characteristic feature is the presence of two peaks at about 764 and 702 cm^{-1}. They are attributed to monosubstituted benzene ring C—H stretching vibration.[33] A strong and wide band appears around 3434 and 3420 cm^{-1} (for PSMA, PSMA-Na and PSMA-RE, respectively), which is assigned to the O—H stretching vibrations of the moisture from the polymer network. Comparing to PSMA, two strong absorption peaks at about 1410, 1415, 1419, 1420, 1424 (for Na^+, La^{3+}, Eu^{3+}, Tb^{3+}, and Yb^{3+}, respectively) and 1570, 1547, 1550, 1551, 1557 cm^{-1} (for Na^+, La^{3+}, Eu^{3+}, Tb^{3+}, and Yb^{3+}, respectively) are corresponding to the COO^- symmetric vibration absorption and asymmetric vibration absorption.[34] Furthermore, $\Delta v_{as\text{-}s}$ ($v_{as} - v_s$) of the PSMA-RE around 133 cm^{-1}, which is smaller than the PSMA-Na ($\Delta v_{as\text{-}s}$ = 160 cm^{-1}). This indicates that the carboxylic groups is a bidentate ligand coordinated to the RE^{3+}.[35] Two bands of PSMA appear at 1856 and 1779 cm^{-1}, which almost disappeared in the complexes (PSMA-RE) due to hydrolysis of anhydride. The results indicated that rare earths ions have been combined with the PSMA resin.

The surface morphologies of PSMA, PSMA-Na, and PSMA-RE are shown in Figure 2(a–f). The image of PSMA sample [Figure 2(a)] exhibits clusters of flowers morphology with a rough surface. After hydrolysis, the agglomerated polymer long-chain have been expanded and the surface morphology becomes coarser than before [shown in Figure 2(b)], which has the large specific surface area, thus benefitting to metal adsorption. In Figure 2(c–f), the surface morphologies of samples PSMA-La, PSMA-Eu, PSMA-Tb, and PSMA-Yb are similar, forming irregular big granules. The average particles diameters of them are above 8 μm. The large sizes make them separate easily from aqueous solution.

In order to elucidate the adsorption mechanism, XPS spectra is applied to characterize the changes of functional groups on adsorbent. In Fig. 3, the presence of La $3d_{5/2}$ (837.45 eV), Eu $3d_{5/2}$ (1135 eV), Tb $3d_{3/2}$ and $3d_{5/2}$ (1241.9 and 1277 eV) and Yb $4d_{5/2}$ (191.5 eV) on the surface of PSMA clearly confirmed the successful adsorption of rare earth ions. O 1s of the PSMA resin is at 532.7 eV. This reflected the chemical structure of anhydride group. After hydrolysis, O 1s shift to a lower binding energy, showing 531.4 eV, which indicated that anhydride group changed COO^- structure. O 1s of the PSMA-RE are at 531.4, 531.6, 531.65, and 531.45 eV (for La, Eu, Tb, and Yb, respectively), which is similar to PSMA-Na. It implied rare earth species combined with the COO^- (Scheme 1).

Adsorption Kinetics

Adsorption kinetics represents the adsorption mechanism and rate-controlling processes. Many scholars studied the adsorption kinetic models for the adsorption of heavy metal ions.[36–39] The adsorption q_t of RE^{3+} as a function of the time t for the hydrolyzed PSMA are depicted in Figure 4. Within the initial 30 min, the adsorption could reach the equilibrium. In present work, adsorption kinetic data were fit by pseudo-first-order and pseudo-second-order equations (6) and (7):

$$\ln(q_e - q_t) = \ln q_e - k_1 t \quad (6)$$

$$\frac{t}{q_t} = \frac{1}{k_2 q_e^2} + \frac{t}{q_e} \quad (7)$$

where q_e and q_t (mg g^{-1}) are the amount of adsorbed RE^{3+} at equilibrium and at time t, respectively, and k_1 (min^{-1}) is the

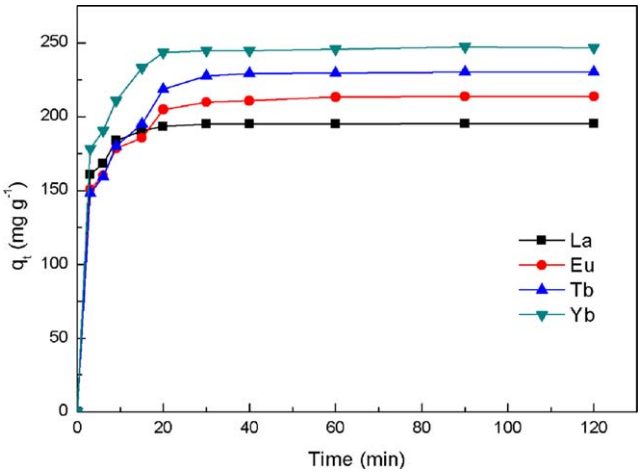

Figure 4. Effect of contact time on the uptakes of La^{3+}, Eu^{3+}, Tb^{3+}, and Yb^{3+} at 298.15 K. [Color figure can be viewed in the online issue, which is available at wileyonlinelibrary.com.]

pseudo-first-order kinetic constant. k_2 (g mg^{-1} min^{-1}) is the pseudo-second-order-rate constant.

The polt of t/q versus t aligned in straight lines (Figure 5), and k_2 and q_e can be determined from the slope and intercept (shown in Table I). From the slope and intercept of the plot of ln (q_e – q_t) versus t, k_1, and q_e can be calculated. Base on the correlation coefficients (R^2), the pseudo-second-order equations fitted the experiment data better than the pseudo-first-order equation, and the experimental data [$q_{e(exp)}$] were 195.3, 213.7, 230.2, and 247.4 mg g^{-1} for La^{3+}, Eu^{3+}, Tb^{3+}, and Yb^{3+}, respectively, shown good agreement with the calculated value according to pseudo-second-order equation. It confirmed that chemical adsorption was the rate-determining step.

Adsorption Isotherm

Adsorption isotherms can provide information about the adsorbate concentration at the surface of adsorbent and in the solution, thereby can reveal the capacity and properties of the adsorbent when the adsorption systems are in equilibrium.[40] The equilibrium isotherms for the adsorption of RE^{3+} on to hydrolyzed PSMA at diffident temperatures (298, 308, and 318 K) at pH of 6.0 are depicted in Figure 6. With increasing temperature, the adsorption capacities of PSMA for RE^{3+} decreased. Temperature is not favorable to adsorption. The equilibrium data was simulated by the Langmuir and Freundlich models at 298.15 K. They are expressed as (8) and (9):

$$\frac{C_e}{q_e} = \frac{C_e}{q_{\max}} + \frac{1}{bq_{\max}} \tag{8}$$

$$\ln q_e = \ln K_F + \frac{1}{n} \ln C_e \tag{9}$$

where b (L mg^{-1}) is the Langmuir constant, $q_{\max}$ (mg g^{-1}) represents the maximum adsorption amount. K_F and n are Freundlich constants related to adsorption capacity and adsorption intensity, respectively.

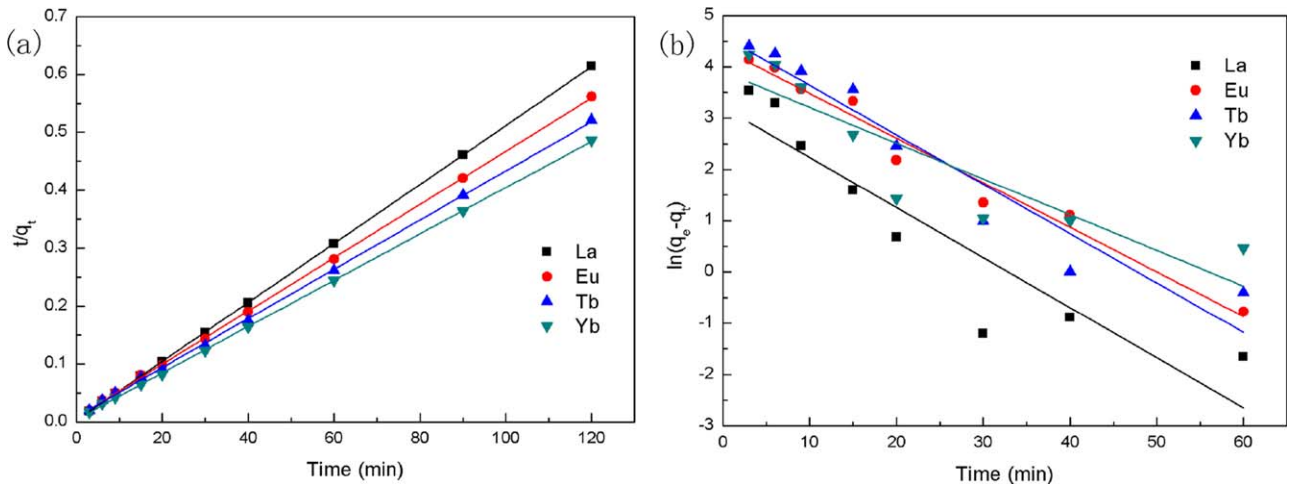

Figure 5. Pseudo-second-order kinetic model (a) and pseudo-first-order kinetic model (b) for adsorption of La^{3+}, Eu^{3+}, Tb^{3+}, and Yb^{3+} on to PSMA. [Color figure can be viewed in the online issue, which is available at wileyonlinelibrary.com.]

Table I. Kinetic Parameters for the Adsorption of La^{3+}, Eu^{3+}, Tb^{3+}, and Yb^{3+} by the PSMA Resin at 298.15 K

Metal	$q_{e(exp)}$ (mg g^{-1})	Pseudo-first-order model			Pseudo-second-order model		
		$q_{e(cal)}$ (mg g^{-1})	k_1 (min^{-1})	R^2	$q_{e(cal)}$(mg g^{-1})	k_2 (g mg^{-1} min^{-1})	R^2
La^{3+}	195.3	24.8	0.09761	0.8513	196.5	9.42×10^{-3}	1.000
Eu^{3+}	213.7	77.4	0.08695	0.9755	217.4	2.79×10^{-3}	0.9998
Tb^{3+}	230.2	99.6	0.09633	0.9252	235.3	2.07×10^{-3}	0.9996
Yb^{3+}	247.4	49.7	0.06972	0.8081	250.0	3.46×10^{-3}	0.9999

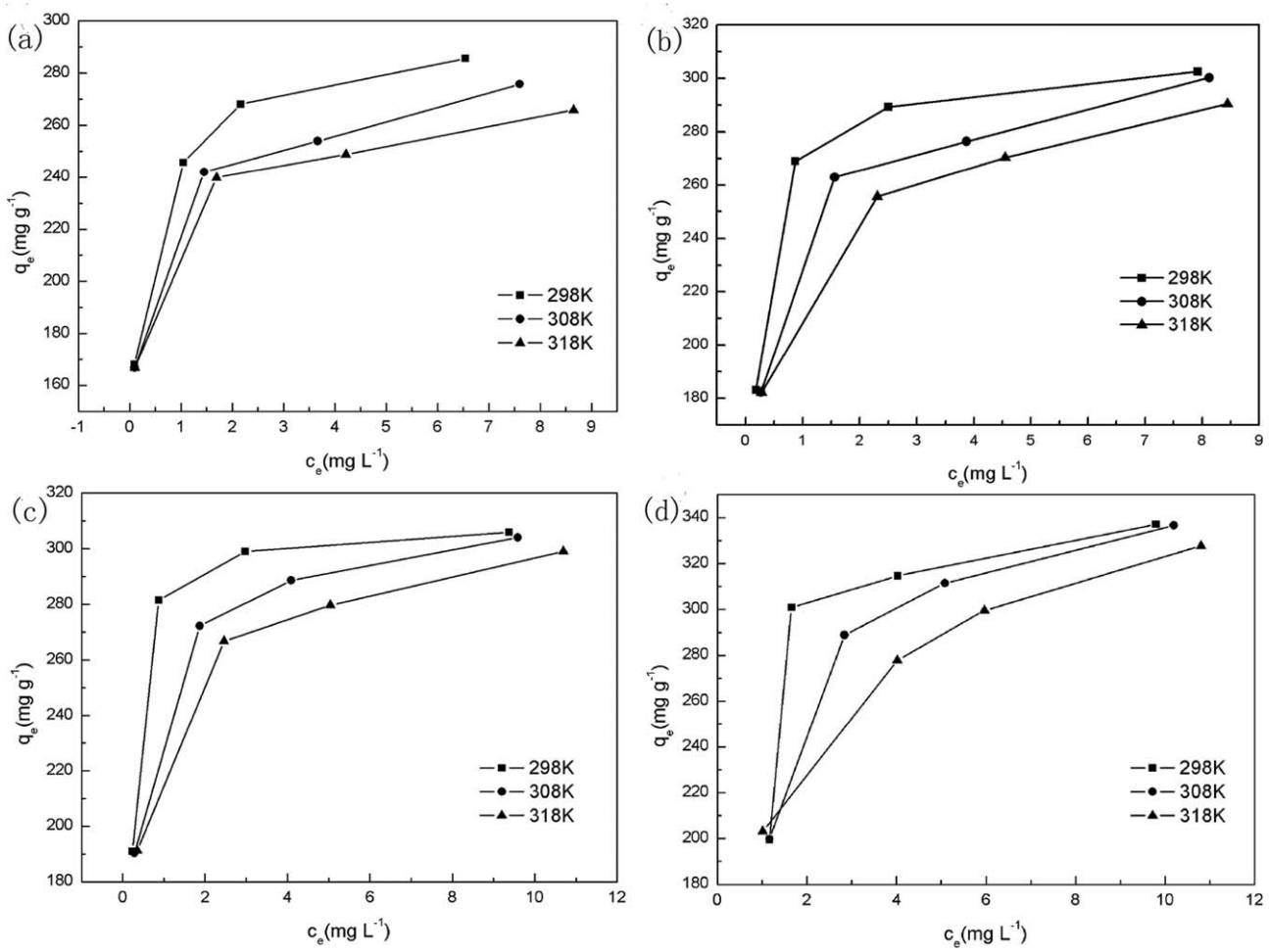

Figure 6. Adsorption isotherms of La^{3+} (a), Eu^{3+} (b), Tb^{3+} (c), and Yb^{3+} (d) on to PSMA at different temperatures.

The results of adsorption isotherm obtained through linear regression procedures are shown in Fig. 7 and Table II. It could be seen that the Langmuir isotherms model was suitable with the experimental data and its correlation coefficients (R^2 = 0.9666, 1, 1 and 0.9959 for La^{3+}, Eu^{3+}, Tb^{3+}, and Yb^{3+}, respectively) were larger than the correlation coefficients of the Freundlich model (R^2 = 0.9666, 0.8562, 0.7670 and 0.6141 for La^{3+}, Eu^{3+}, Tb^{3+}, and Yb^{3+}, respectively). The Langmuir isotherms model indicated that the adsorbed RE^{3+} formed monolayer coverage on the adsorbent surface. According to Langmuir

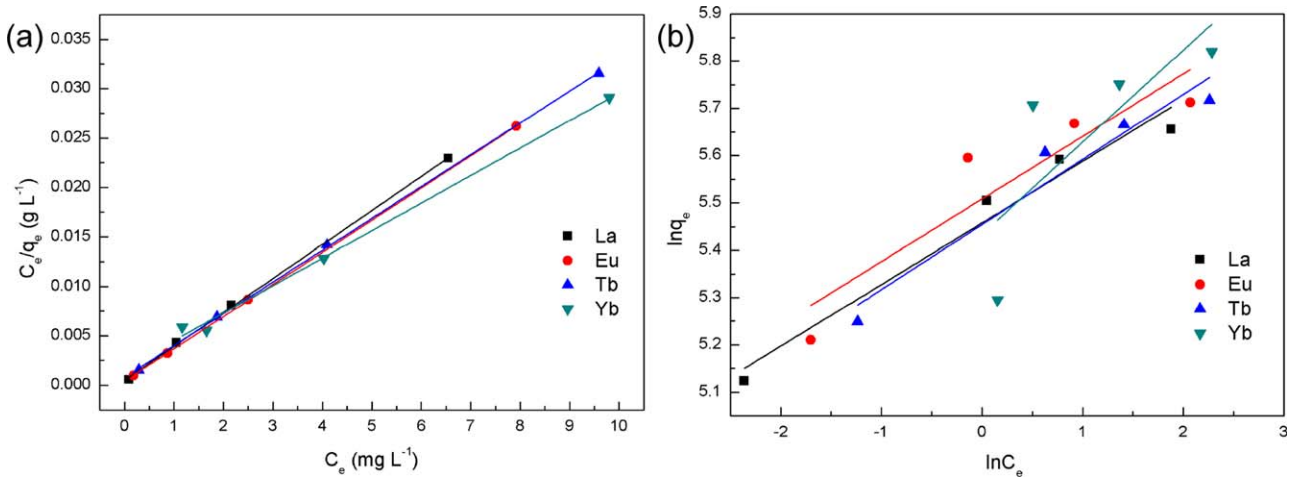

Figure 7. Langmuir (a) and Freundlich (b) isotherms for the adsorption of La^{3+}, Eu^{3+}, Tb^{3+}, and Yb^{3+} on to the PSMA resin at 298.15 K. [Color figure can be viewed in the online issue, which is available at wileyonlinelibrary.com.]

Table II. Isotherm Parameters for the Adsorption of La^{3+}, Eu^{3+}, Tb^{3+}, and Yb^{3+} by the PSMA Resin at 298.15 K

	Parameter	La^{3+}	Eu^{3+}	Tb^{3+}	Yb^{3+}
	$q_{e(exp)}$ (mg g^{-1})	285.79	301.92	305.46	336.65
	q_{max} (mg g^{-1})	290.70	307.69	309.60	359.71
Langmuir	b (L mg^{-1})	7.0558	7.4898	8.5896	1.6069
	R^2	0.9996	1	1	0.9959
Freundlich	K_F	234.58	246.73	250.96	228.95
	N	7.6746	7.5586	8.1766	5.1282
	R^2	0.9666	0.8562	0.7670	0.6141

isotherm equation, the maximum adsorption capacities (q_{max} = 290.70, 307.69, 309.60 mg g^{-1} and 359.71 for La^{3+}, Eu^{3+}, Tb^{3+}, and Yb^{3+}, respectively) of hydrolyzed PSMA were close to the experimental value [$q_{e(exp)}$ = 285.79, 301.92, 305.46 and 336.65 mg g^{-1} for La^{3+}, Eu^{3+}, Tb^{3+}, and Yb^{3+}, respectively], which is much better than that Ponou *et al.* and Iannicelli-Zubiani *et al.* reported.[41,42]

The thermodynamic properties of rare earth ions adsorption can be reflected by thermodynamic parameters, such as Gibbs free energies change (ΔG), enthalpy change (ΔH) and entropy change (ΔS). They can be calculated using eqs. (10) and (11):

$$\Delta G = -RT \ln K_d \quad (10)$$

$$\ln K_d = \frac{\Delta S}{R} - \frac{\Delta H}{RT} \quad (11)$$

where R is gas constant (8.314 J mol^{-1} K^{-1}), T is the system temperature (K), and K_d is the distribution coefficient.

The thermodynamic parameters for the adsorption process of rare earth ions on the PSMA resin are shown in Table III. The negative values of ΔG and ΔH for all metal ions implied that the adsorption was spontaneous exothermic process, confirming that adsorption was favored by decreasing temperature. Moreover, the positive ΔS revealed the degrees of freedom increases at the adsorbent–adsorbate interface during the adsorption process. It is well-known that $RE(H_2O)_n^{3+}$ ($n > 8$) as the most common chemical forms exists in aqueous solution. When the complexes (PSMA-RE) formed, each metal ion was bonded to three carboxylic groups and water molecules left. Thus, particle numbers increase in system, leading to entropy increase.[43]

Table III. Thermodynamic Parameters for the Adsorption of RE (III) Ions on to PSMA

Metal	T (K)	ΔG (kJ mol^{-1})	ΔH (kJ mol^{-1})	ΔS (J mol^{-1} K^{-1})
La^{3+}	298.15	−16.216	−3.786	41.7400
	308.15	−16.666		
	318.15	−17.049		
Eu^{3+}	298.15	−15.611	−12.524	10.0599
	308.15	−15.434		
	318.15	−15.825		
Tb^{3+}	298.15	−15.309	−16.351	3.5966
	308.15	−15.184		
	318.15	−15.241		
Yb^{3+}	298.15	−13.288	−5.954	24.3384
	308.15	−13.280		
	318.15	−13.786		

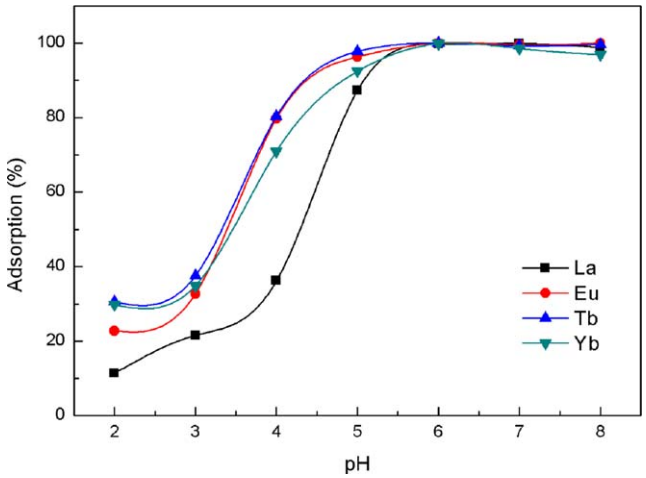

Figure 8. Effect of pH on La^{3+}, Eu^{3+}, Tb^{3+}, and Yb^{3+} adsorption by PSMA resin. [Color figure can be viewed in the online issue, which is available at wileyonlinelibrary.com.]

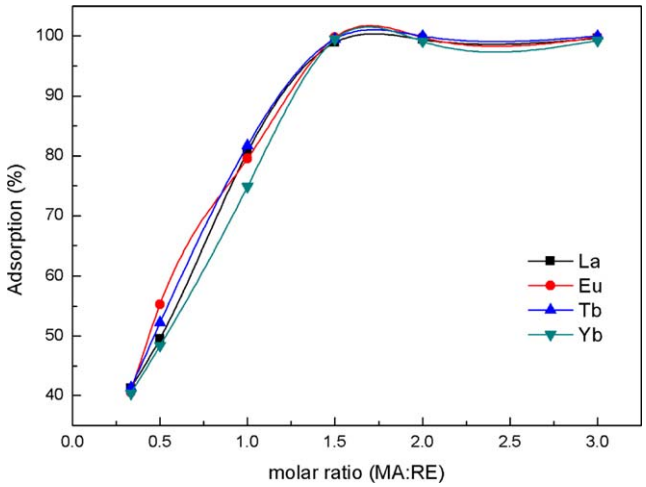

Figure 9. Effect of the molar ratio on the adsorption of La^{3+}, Eu^{3+}, Tb^{3+}, and Yb^{3+} on to PSMA. [Color figure can be viewed in the online issue, which is available at wileyonlinelibrary.com.]

Table IV. Effect of Interfering Ions on the Adsorption of La^{3+}, Eu^{3+}, Tb^{3+}, and Yb^{3+}

	Interfering ions	Content ratio	Adsorption of RE^{3+} (%)	β	Residual amount of RE (mg L^{-1})
La^{3+}	Ca^{2+}	5:1	98.26	1.03×10^3	0.3428
	Mg^{2+}	2.5:1	92.96	0.26×10^3	0.3660
Eu^{3+}	Ca^{2+}	5:1	99.86	1.04×10^4	0.0275
	Mg^{2+}	2.5:1	99.97	3.57×10^4	0.0069
Tb^{3+}	Ca^{2+}	5:1	99.71	2.28×10^3	0.0559
	Mg^{2+}	2.5:1	99.52	2.29×10^3	0.0948
Yb^{3+}	Ca^{2+}	5:1	99.37	5.21×10^3	0.1221
	Mg^{2+}	2.5:1	99.78	4.38×10^3	0.0441

Table V. Desorption of La^{3+}, Eu^{3+}, Tb^{3+}, and Yb^{3+} from Metal-Loaded PSMA Using HCl with Different Concentration

	Stripping reagent	La^{3+}	Eu^{3+}	Tb^{3+}	Yb^{3+}
Desorption (%)	0.1 mol L^{-1} HCl	30.36	36.26	48.59	26.97
	0.5 mol L^{-1} HCl	92.25	95.62	96.83	91.79
	1 mol L^{-1} HCl	99.46	99.39	99.19	99.30

Effect of pH, Adsorbent Dose, and Interfering Ions

In the adsorption procedure, pH has been reported as a key condition because it controls the surface charge and the ionization degree of the adsorbent.[38] A series of batch equilibrium tests were carried out in the range of 2–8. In Figure 8, the percentage of RE^{3+} adsorption increased at pH range of 2.0–6.0 and then almost kept equilibrium at higher pH. We can observe the lower percentage of RE^{3+} adsorption at pH 2.0 which may be attributed to the protonation of carboxyl group and the hydrogen band formed between the chains. This resultant caused reducing amount of active groups and weak coordination with RE(III) ions. For pH 6, carboxyl group was ionized and the percentage of RE^{3+} adsorption reached a maximum value. When pH value was higher than 6.0, the percentage of RE^{3+} adsorption did not change obviously. The rare earth hydroxides were formed and began to precipitate in sulfate solution.[44] Thereby the pH value of 6.0 was selected as optimum condition.

The adsorbent dose is another important parameter. It determined the amount of active sites for adsorption process. We used the different molar rate of MA to rare earth ions for investigating the effect of adsorbent dose on the adsorption. As shown in Figure 9, the percentage of RE^{3+} adsorption increased with increasing adsorbent dose and reached saturation when the molar rate of MA to rare earth ions is about 1.5:1. The percentage of adsorption approached to 98.89, 99.76, 99.5, and 99.45% for La^{3+}, Eu^{3+}, Tb^{3+}, and Yb^{3+}, respectively, and then increased slightly with adsorbent dose increasing. Therefore, the optimum molar ratio on the adsorption was selected 1.5:1 (MA:RE^{3+}).

In traditional hydrometallurgical process for rare earths, the thorium and fluorine as impurities are removed from the sulfate/chloride leaching solution by precipitation with the addition of a calcium/magnesium salt.[26] Therefore, the Ca^{2+} and Mg^{2+} were chosen for the competitive experiment. The adsorption in a two-component system was investigated using a molar ratio of 2:1 (MA:RE^{3+}) (Table IV). When Mg^{2+} or Ca^{2+} was added, the adsorption efficiency of rare earth ions had no obvious change and the values of β were much bigger than 1. While the residual amount of RE was lower than 0.4 mg L^{-1} in the solution, reaching effluent standard of GB. The results indicated that the PSMA resins performed an excellent selectivity for rare earth ions.

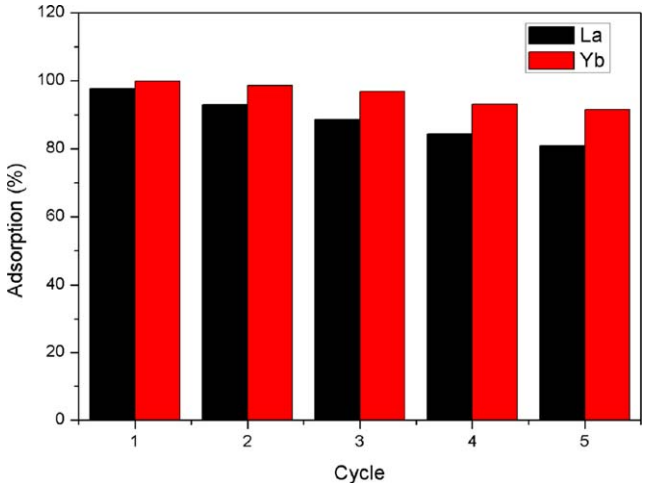

Figure 10. Recycling of the PSMA resin in the adsorption of La^{3+} and Yb^{3+}. [Color figure can be viewed in the online issue, which is available at wileyonlinelibrary.com.]

Desorption and Regeneration Studies

Desorption performance and reusability are important characters for an adsorbent, which influence on the potential practical application and economic effectiveness. We used HCl as a stripping reagent. The results (Table V) show that the desorption efficiencies of La^{3+}, Eu^{3+}, Tb^{3+}, and Yb^{3+} were 99.46, 99.39, 99.19, and 99.30%, indicating that 1 mol L^{-1} HCl is the optimal desorption condition for rare earth ions. And then the desorbed PSMA resin was regenerated in 0.02 mol L^{-1} NaOH. Figure 10 presents the adsorption efficiency of La^{3+} and Yb^{3+} over five successive adsorption–desorption cycles. It was observed that approximate 97.72 and 99.89% of adsorption efficiency were reached in the first cycle for La^{3+} and Yb^{3+}, respectively, and 80.79 and 91.5% of adsorption efficiency were still retained at the end of the fifth cycle.

CONCLUSIONS

In this study, we presented that the hydrolyzed PSMA showed excellent adsorption performance for rare earth ions due to the functional groups (COO^-) on the chains of hydrolyzed PSMA. The maximum adsorption capacity of La^{3+}, Eu^{3+}, Tb^{3+}, and Yb^{3+} is 285.79, 301.92, 305.46, and 336.65 mg g^{-1} at 298 K and pH 6.0. The adsorption process is accomplished in 30 min. The IR and XPS survey results revealed that RE^{3+} coordinated with COO^- in PSMA after adsorption. The experimental data were well fitted by pseudo-second-order kinetics model and Langmuir isotherm. The competitive study demonstrated that the effect of common coexisting ions on RE^{3+} removal was negligible. Moreover, the rare earth ions were desorbed by 1 mol L^{-1} HCl solution and the adsorbent could be efficiently regenerated by NaOH. The results suggested that the hydrolyzed PSMA resin has great application prospects in dealing with wastewater containing rare earth ions.

ACKNOWLEDGMENTS

This project is supported by the National Natural Science Foundation of China (No. 51474118) and the Personnel Training Program of National Basic Research of China (No. J1103307).

REFERENCES

1. Humphries, M. Rare Earth Element: The Global Supply Chain; Congressional Research Service **2013**, p 3.
2. Binnemansetal, K. *J. Clean. Prod.* **2013**, *51*, 1.
3. Hirano, S.; Suzuki, K. T. *Environ. Health Perspect.* **1996**, *104*, 85.
4. Chen, Z. Y.; Zhu, X. D. *J. Ecol. Rural Environ.* **2008**, *24*, 88.
5. Pałasz, A.; Czekaj, P. *Acta Biochim. Polym.* **2000**, *47*, 1107.
6. Byers, C. H.; Williams, D. F. *Indus. Eng. Chem. Res.* **1996**, *35*, 993.
7. Li, C.; Zhuang, Z.; Huang, F.; Wu, Z.; Hong, Y.; Lin, Z. *ACS Appl. Mater. Interfaces* **2013**, *5*, 9719.
8. Yin, S.; Wu, W.; Bian, X.; Luo, Y.; Zhang, F. *Indus. Eng. Chem. Res.* **2013**, *52*, 8558.
9. Wang, W.; Yang, H.; Cui, H.; Zhang, D.; Liu, Y.; Chen, J. *Indus. Eng. Chem. Res.* **2011**, *50*, 7534.
10. Yadav, K. K.; Singh, D. K.; Anitha, M.; Varshney, L.; ; Singh, H. *Sep. Purif. Technol.* **2013**, *118*, 350.
11. Tian, M.; Jia, Q.; Song, N.; Quan, X.; Liu, C. *J. Chem. Eng. Data* **2010**, *55*, 4281.
12. Sui, N.; Huang, K.; Zhang, C.; Wang, N.; Wang, F.; Liu, H. *Indus. Eng. Chem. Res.* **2013**, *52*, 5997.
13. Jia, Q.; Shang, Q.; Zhou, W. *Indus. Eng. Chem. Res.* **2004**, *43*, 6703.
14. Pietrelli, L.; Bellomo, B.; Fontana, D.; Montereali, M. R. *Hydrometallurgy* **2002**, *66*, 135.
15. Shimizu, K.; Kuribayashi, H.; Watanabe, H.; Shimasaki, T.; Azuma, K.; Horie, Y.; Saitoh, K.; Saito, S.; Shibukawa, M. *Anal. Chem.* **2013**, *85*, 978.
16. Krättli, M.; Müller-Späth, T.; Ulmer, N.; Ströhlein, G.; Morbidelli, M. *Indus. Eng. Chem. Res.* **2013**, *52*, 8880.
17. Park, H.; ; Tavlarides, L. L. *Indus. Eng. Chem. Res.* **2010**, *49*, 12567.
18. Amarasekara, A. S.; Owereh, O. S.; Aghara, S. K. *J. Rare Earth Met.* **2009**, *27*, 870.
19. Takahashi, Y.; Châtellier, X.; Hattori, K. H.; Kato, K.; Fortin, D. *Chem. Geol.* **2005**, *219*, 53.
20. Abdel-Rehim, A. M. *Hydrometallurgy* **2002**, *67*, 9.
21. Qu, R.; Sun, C.; Zhang, Y.; Chen, J.; Wang, C.; Ji, C.; ; Liu, X. *J. Chem. Eng. Data* **2010**, *55*, 4343.
22. Akkaya, R. *Chem. Eng. J.* **2012**, *200–202*, 186.
23. Zheng, X.; Wu, D.; Su, T.; Bao, S.; Liao, C.; Wang, Q. *ACS Appl. Mater. Interfaces* **2014**, *6*, 19840.
24. Gui, W.; Zhang, H.; Liu, Q.; Zhu, X.; Yang, Y. *Hydrometallurgy* **2014**, *147–148*, 157.
25. Kul, M.; Topkaya, Y.; Karakaya, İ. *Hydrometallurgy* **2008**, *93*, 129.
26. Wang, L.; Yu, Y.; Huang, X.; Long, Z.; Cui, D. *Chem. Eng. J.* **2013**, *215–216*, 162.
27. Wu, W.; Bian, X. Metallurgy Technology of Rare Earth; 1st ed.; Science Press: Beijing, China, **2012**, p 37.
28. Liang, X.; Su, Y.; Yang, Y.; Qin, W. *J. Hazard. Mater.* **2012**, *203–204*, 183.
29. Ren, H.; Lang, H. Q. Handbook of Analytical Chemistry; Chemical Industry Press: Beijing, China, **1997**, p 26.
30. Xiong, C.; Li, Y.; Wang, G.; Fang, L.; Zhou, S.; Yao, C.; Chen, Q.; Zheng, X.; Qi, D.; Fu, Y.; Zhu, Y. *Chem. Eng. J.* **2015**, *259*, 257.
31. Cegłowski, M.; Schroeder, G. *Chem. Eng. J.* **2015**, *259*, 885.
32. Chen, Y.; He, M.; Wang, C.; Wei, Y. *J. Mater. Chem. A* **2014**, *2*, 10444.
33. Qi, X. Spectrum Method in the Study of Organic and Polymer Structure; Science Press: Beijing, China, **2011**, p 60.
34. Chang, J.; Dong, Q. Spectrum Principle and Parsing; Science Press: Beijing, China, **2005**, p 89.
35. Nakamoto, K. Infrared and Raman Spectra of Inorganic and Coordination Compounds, 4th ed.; Wiley: New York, **1986**.

36. Cegłowski, M.; Schroeder, G. *Chem. Eng. J.* **2015**, *263*, 402.
37. Zhang, S.; Shu, X.; Zhou, Y.; Huang, L.; Hua, D. *Chem. Eng. J.* **2014**, *253*, 55.
38. Tang, L.; Fang, Y.; Pang, Y.; Zeng, G.; Wang, J.; Zhou, Y.; Deng, Y.; Yang, G.; Cai, Y.; Chen, J. *Chem. Eng. J.* **2014**, *254*, 302.
39. Chen, H.; Shao, D.; Li, J.; Wang, X. *Chem. Eng. J.* **2014**, *254*, 623.
40. Hong, G.; Shen, L.; Wang, M.; Yang, Y.; Wang, X.; Zhu, M.; Hsiao, B. S. *Chem. Eng. J.* **2014**, *244*, 307.
41. Ponoua, J.; Wang, L.; Dodbiba, G.; Okaya, K.; Fujita, T.; Mitsuhashi, K.; Atarashi, T.; Satoh, G.; Noda, M. *J. Environ. Chem. Eng.* **2014**, *2*, 1070.
42. Iannicelli-Zubiani, E. M.; Cristiani, C.; Dotelli, G.; Stampino, P. G.; Pelosato, R.; Mesto, E.; Schingaro, E.; Lacalamita, M. *Waste Manage.* **2015**, *46*, 546.
43. Zhang, R. Y. Rare Earth Element Chemistry, 1st ed.; Tianjin Science and Technology Press: Tianjin, China, **1987**, p 206.
44. Sun Yat-Sen University Department of Metal Editor; Rare Earth Physical and Chemical Constants; Metallurgy Industry Press: Beijing, **1978**, p 81.